

A Comparison Between Invariant and Equivariant Classical and Quantum Graph Neural Networks

Roy T. Forestano

IFT, Department of Physics
University of Florida
Gainesville, FL 32611
roy.forestano@ufl.edu

Marçal Comajoan Cara

Department of Signal Theory and Communications
Polytechnic University of Catalonia
Barcelona, Barcelona 08034, Spain
marcal.comajoan@estudiantat.upc.edu

Gopal Ramesh Dahale

Indian Inst. of Technology Bhilai
Kutelabhata, Khapri,
Chhattisgarh – 491001, India
gopald@iitbhillai.ac.in

Zhongtian Dong

Dep. Physics & Astronomy
University of Kansas
Lawrence, KS 66045
cosmos@ku.edu

Sergei Gleyzer

Dep. Physics & Astronomy
University of Alabama
Tuscaloosa, AL 35487
sgleyzer@ua.edu

Daniel Justice

Software Engineering Institute
Carnegie Mellon University
Pittsburgh, PA 15213
dljustice@sei.cmu.edu,

Kyoungchul Kong

Dep. Physics & Astronomy
University of Kansas
Lawrence, KS 66045
kckong@ku.edu

Tom Magorsch

Physik-Department
Technische Univ. München
85748 Garching, Germany
tom.magorsch@tum.de

Konstantin T. Matchev

IFT, Physics Department,
University of Florida
Gainesville, FL 32611
matchev@ufl.edu

Katia Matcheva

IFT, Physics Department,
University of Florida
Gainesville, FL 32611
matcheva@ufl.edu

Eyup B. Unlu

IFT, Physics Department,
University of Florida
Gainesville, FL 32611
eyup.unlu@ufl.edu

Abstract

Machine learning algorithms are heavily relied on to understand the vast amounts of data from high-energy particle collisions at the CERN Large Hadron Collider (LHC). The data from such collision events can naturally be represented with graph structures. Therefore, deep geometric methods, such as graph neural networks (GNNs), have been leveraged for various data analysis tasks in high-energy physics. One typical task is jet tagging, where jets are viewed as point clouds with distinct features and edge connections between their constituent particles. The increasing size and complexity of the LHC particle datasets, as well as the computational models used for their analysis, greatly motivate the development of alternative fast and efficient computational paradigms such as quantum computation. In addition, to enhance the validity and robustness of deep networks, one can leverage the fundamental symmetries present in the data through the use of invariant inputs and equivariant layers. In this paper, we perform a fair and comprehensive comparison between classical graph neural networks (GNNs) and equivariant graph neural networks (EGNNs) and their quantum counterparts: quantum graph neural networks (QGNNs) and equivariant quantum graph neural networks (EQGNN). The four architectures were benchmarked on a binary classification task to classify the parton-level particle initiating the jet. Based on their AUC scores, the quantum networks were shown to outperform the classical networks. However, seeing the

computational advantage of the quantum networks in practice may have to wait for the further development of quantum technology and its associated APIs.

1 Introduction

Through the measurement of byproducts of particle collisions, the Large Hadron Collider (LHC) collects a substantial amount of information about the fundamental particles and their interactions. The data produced from these collisions can be analyzed using various supervised and unsupervised machine learning methods [2, 32, 23, 24, 22]. Jet tagging is a key task in high energy physics which seeks to identify the likely parton-level particle from which the jet originated. By viewing individual jets as point clouds with distinct features and edge connections between the constituent particles which make them up, a graph neural network (GNN) has been considered as a well-suited architecture for jet tagging [23, 32].

Classified as deep geometric networks, GNNs have the potential to draw inferences about a graph structure, including the interactions among elements in the graph [36, 41]. Graph neural networks are typically thought of as generalizations of convolutional neural networks (CNNs), which are predominantly used for image recognition, pattern recognition, and computer vision [15, 16]. This can be attributed to the fact that, in an image, each pixel is connected to its nearest neighboring pixels, whereas in a general dataset, one would ideally like to construct an arbitrary graph structure among the samples. Many instances in nature can be described well in terms of graphs, including molecules, maps, social networks, and the brain. For example, in molecules, the nodal data can be attributed to the atoms, the edges can be characterized as the strength of the bond between atoms, and the features embedded within each node can be the atom characteristics, such as the reactivity.

Generally, graphically-structured problems involve unordered sets of elements with learnable embedding of the input features. Useful information can be extracted from such graph structured data by the embedding it within GNNs. Many subsequent developments have been made to progress GNNs since their first implementation in 2005, including graph convolutional, recurrent, message passing, graph attention, and graph transformer, architectures [36, 32, 14, 37].

To enhance the validity and robustness of deep networks, invariant and equivariant networks have been constructed to learn the symmetries embedded within a dataset by preserving an oracle in the former and by enforcing weight sharing across filter orientations in the latter [18, 7]. Utilizing analytical invariant quantities characteristic of physical symmetry representations, computational methods have successfully rediscovered fundamental Lie group structures, such as the $SO(n)$, $SO(1, 3)$, and $U(n)$ groups [10, 12, 11, 9]. Non-linear symmetry discovery methods have also been applied across classification tasks in data domains [29]. The simplest and most useful embedded symmetry transformations include translations, rotations, and reflections, which have been the primary focus in invariant (IGNN) and equivariant graph neural networks (EGNN) [19, 30].

The learned representations from the collection of these network components can be used to understand unobservable causal factors, uncover fundamental physical principles governing these processes, and possibly even discover statistically significant hidden anomalies. However, with increasing amounts of available data and the computational cost of these deep learning networks, large computing resources will be required to efficiently run these machine learning algorithms. The extension of classical networks, which relies on bit-wise computation, to quantum networks, which relies on qubit-wise computation, is already underway as a solution to this complexity problem. Many APIs, including Xanadu’s PennyLane, Google’s Cirq, and IBM’s Qiskit, have been developed to allow for the testing of quantum circuits and quantum machine learning algorithms running on these quantum devices. In the quantum graph structure, classical nodes can be mapped to quantum states, real valued features to the complex valued characteristics of the states, edges to the interactions between states, and edge attributes to the strength of the interactions between the quantum states. Through a well-defined Hamiltonian operator, the larger structure of a classical model can then be embedded into the quantum model. This parameterized Hamiltonian determines the evolution of the quantum system by acting on the quantum states within the graph. Following several layers of application, a final state measurement of the quantum system can then be made to reach a final prediction. The theory and application of unsupervised and supervised learning tasks involving quantum graph neural networks (QGNNs), quantum graph recurrent neural networks (QGRNNs), and quantum graph convolutional neural networks (QGCNNs) have already been developed [3, 38]. Improvements

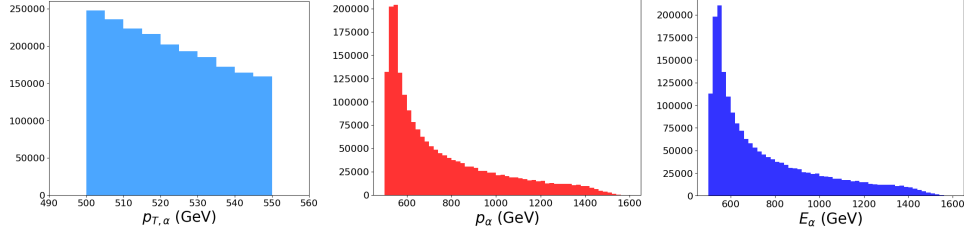


Figure 1: Distributions of the jet transverse momenta p_T , total momenta p , and energies E .

of these models to arbitrarily sized graphs have been made with the implementation of ego-graph based quantum graph neural networks (egoQGNN) [1]. Quantum analogs of other advanced classical architectures, including generative adversarial networks (GANs), transformers, natural language processors (NLPs), and equivariant networks, have also been proposed [3, 27, 5, 33, 4, 21, 26, 31].

With the rapid development of quantum deep learning, this work intends to offer a fair and comprehensive comparison between GNNs and their quantum counterparts. To classify whether a particle jet has originated from a quark or a gluon, a binary classification task was carried out across four different architectures. These architectures include a GNN, SE(2) EGNN, QGNN, and permutation EQGNN. Each quantum model was fine tuned to have an analogous structure to its classical form. In order to provide a fair comparison, all models used similar hyperparameters, as well as a similar number of total trainable parameters. The final results across each architecture using identical training, validation, and testing sets were recorded. We find that the QGNN and EQGNN outperform their classical analogs on the particular binary classification task described above. Although these results seem promising for the future of quantum computing, further development of quantum application programming interfaces (APIs) is required to allow for more general implementations of quantum architectures.

2 Data

The jet-tagging binary classification task is illustrated with the high energy physics (HEP) dataset *Pythia8 Quark and Gluon Jets for Energy Flow* [17], which contains two million jets split equally into one million quark jets and one million gluon jets. These jets resulted from LHC collisions with total center of mass energy $\sqrt{s} = 14$ TeV and were selected to have transverse momenta p_T^{jet} between 500 to 550 GeV and rapidities $|y^{jet}| < 1.7$. The jet kinematic distributions are shown in Fig. 1. For each jet α , the classification label is provided as either a quark with $y_\alpha = 1$ or a gluon with $y_\alpha = 0$, and each particle i within the jet is listed with its transverse momentum $p_{T,\alpha}^{(i)}$, rapidity $y_\alpha^{(i)}$, azimuthal angle $\phi_\alpha^{(i)}$, and PDG id $I_\alpha^{(i)}$.

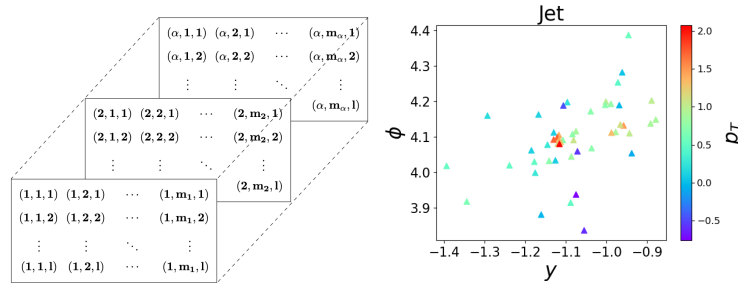


Figure 2: A visualization of graphically structured data (left) and a sample jet shown in the (ϕ, y) plane (right) with each particle color-coded by its transverse momentum $p_{T,\alpha}^{(i)}$.

2.1 Graphically structured data

A graph \mathcal{G} is typically defined as a set of nodes \mathcal{V} and edges \mathcal{E} , i.e. $\mathcal{G} = \{\mathcal{V}, \mathcal{E}\}$. Each node $v^{(i)} \in \mathcal{V}$ is connected to its neighboring nodes $v^{(j)}$ via edges $e^{(ij)} \in \mathcal{E}$. In our case, each jet α can be considered as a graph \mathcal{J}_α composed of the jet's constituent particles as nodes $v_\alpha^{(i)}$ with node features $h_\alpha^{(i)}$ and edge connections $e_\alpha^{(ij)}$ between the nodes in \mathcal{J}_α with edge features $a_\alpha^{(ij)}$. It should be noted that the number of nodes within a graph can vary. This is especially true for the case of particle jets, where the number of particles within each jet can vary greatly. Each jet \mathcal{J}_α can be considered as a collection of m_α particles with l distinct features per particle. An illustration of graphically structured data and an example jet in the (ϕ, y) plane can be seen in Fig. 2.

2.2 Feature engineering

We use the `Particle` package [28] to find the particle masses $m_\alpha^{(i)}$ from the respective particle id's $I_\alpha^{(i)}$. From the available kinematic information for each particle i , we construct new physically meaningful kinematic variables [13], which will be used as additional features in the analysis. In particular, we consider the transverse mass $m_{T,\alpha}^{(i)}$, the energy $E_\alpha^{(i)}$, and the Cartesian momentum components, $p_{x,\alpha}^{(i)}$, $p_{y,\alpha}^{(i)}$, and $p_{z,\alpha}^{(i)}$, defined respectively as

$$m_{T,\alpha}^{(i)} = \sqrt{m_\alpha^{(i)2} + p_{T,\alpha}^{(i)2}}, \quad E_\alpha^{(i)} = m_{T,\alpha}^{(i)} \cosh(y_\alpha^{(i)}), \quad (1a)$$

$$p_{x,\alpha}^{(i)} = p_{T,\alpha}^{(i)} \cos(\phi_\alpha^{(i)}), \quad p_{y,\alpha}^{(i)} = p_{T,\alpha}^{(i)} \sin(\phi_\alpha^{(i)}), \quad p_{z,\alpha}^{(i)} = m_{T,\alpha}^{(i)} \sinh(y_\alpha^{(i)}). \quad (1b)$$

The original kinematic information in the dataset is then combined with the additional kinematic variables (1) into a feature set $h_\alpha^{(il)}$, $l = 0, 1, 2, \dots, 7$, as follows

$$h_\alpha^{(il)} \equiv \left\{ p_{T,\alpha}^{(i)}, y_\alpha^{(i)}, \phi_\alpha^{(i)}, m_{T,\alpha}^{(i)}, E_\alpha^{(i)}, p_{x,\alpha}^{(i)}, p_{y,\alpha}^{(i)}, p_{z,\alpha}^{(i)} \right\}. \quad (2)$$

These features were then max scaled by their maximum value across all jets α and particles i , i.e. $h_\alpha^{(il)} \rightarrow h_\alpha^{(il)} / \max_{\alpha,i}(h_\alpha^{(il)})$.

Edge connections are formed via the Euclidean distance $\Delta R = \sqrt{\Delta\phi^2 + \Delta y^2}$ between one particle and its neighbor in (ϕ, y) space. Therefore, the edge attribute matrix for each jet can be expressed as

$$a_\alpha^{(ij)} \equiv \Delta R_\alpha^{(ij)} = \sqrt{\left(\phi_\alpha^{(i)} - \phi_\alpha^{(j)}\right)^2 + \left(y_\alpha^{(i)} - y_\alpha^{(j)}\right)^2}. \quad (3)$$

2.3 Training, Validation, and Testing Sets

We consider jets with at least 10 particles. This leaves us with $N = 1,997,445$ jets, 997,805 of which are quark jets. While the classical GNN is more flexible in terms of its hidden features, the size of the quantum state and the Hamiltonian scale as 2^n , where n is the number of qubits. As we shall see, the number of qubits will be given by the number of nodes n_α in the graph, i.e. the number of particles in the jet. Therefore, jets with large particle multiplicity will require prohibitively complex quantum networks. This is why, we limit ourselves to the case of $n_\alpha = 3$, and for each jet, only consider the three highest p_T particles. In other words, each graph contains the set $\mathbf{h}_\alpha = (\mathbf{h}_\alpha^{(1)}, \mathbf{h}_\alpha^{(2)}, \mathbf{h}_\alpha^{(3)})$ where each $\mathbf{h}_\alpha^{(i)} \in \mathbb{R}^8$ and $\mathbf{h}_\alpha \in \mathbb{R}^{3 \times 8}$. For training, we randomly picked $N = 12,500$ jets and used the first 10,000 for training, the next 1,250 for validation, and the last 1,250 for testing. These sets happened to contain 4982, 658, and 583 quark jets, respectively.

3 Models

The four different models described below, including a GNN, EGNN, QGNN, and EQGNN, were constructed to perform graph classification. The binary classification task was to determine whether a jet \mathcal{J}_α originated from a quark or a gluon.

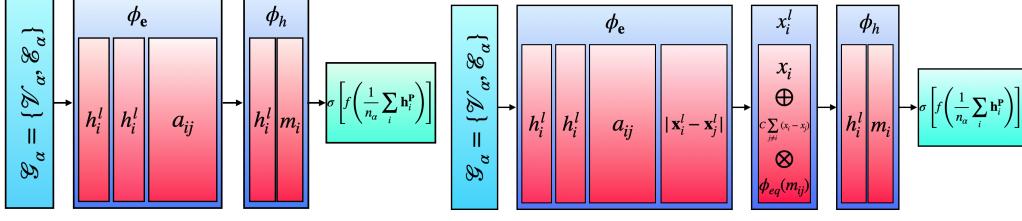


Figure 3: Graph neural network (GNN, left) and equivariant graph neural network (EGNN, right) schematic diagrams.

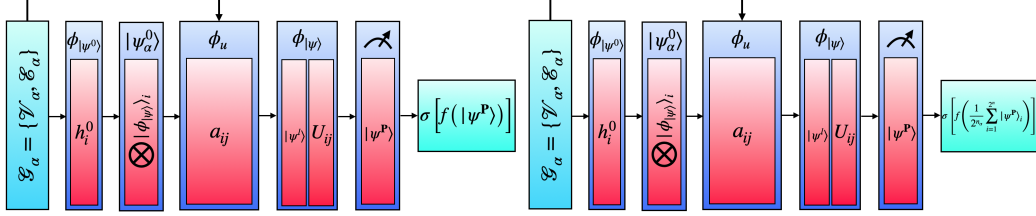


Figure 4: Quantum graph neural network (QGNN, left) and equivariant quantum graph neural network (EQGNN, right) schematic diagrams.

3.1 Invariance and Equivariance

By making a network invariant or equivariant to particular symmetries within a dataset, a more robust architecture can be developed. In order to introduce invariance and equivariance, one must assume or learn a certain symmetry group G of transformations on the dataset. A function $\varphi : X \rightarrow Y$ is equivariant with respect to a set of group transformations $T_g : X \rightarrow X, g \in G$, acting on the input vector space X , if there exists a set of transformations $S_g : Y \rightarrow Y$ which similarly transform the output space Y , i.e.

$$\varphi(T_g x) = S_g \varphi(x). \quad (4)$$

A model is said to be invariant when for all $g \in G$, S_g becomes the set containing only the trivial mapping, i.e. $S_g = \{\mathbb{I}_G\}$, where $\mathbb{I}_G \in G$ is the identity element of the group G [18, 8].

Invariance has been shown to perform better as an input embedding, whereas equivariance can be more easily incorporated into the model layers. For each model, the invariant component corresponds to the translational and rotational invariant embedding distance $\varphi \equiv \Delta R_\alpha^{(ij)}$, where in this case $\varphi : \mathbb{R}^2 \times \mathbb{R}^2 \rightarrow \mathbb{R}$, which makes up the edge attribute matrix $a_\alpha^{(ij)}$, as defined in Eq. 3. This distance is used as opposed to solely incorporating the raw coordinates. Equivariance has been accomplished through the use of simple nontrivial functions along with higher order methods involving the use of spherical harmonics to embed the equivariance within the network [25, 39]. Equivariance takes different forms in each model presented here.

3.2 Graph neural network

Classical GNNs take in a collection of graphs $\{\mathcal{G}_\alpha\}$ each with nodes $v_\alpha^{(i)} \in \mathcal{V}_\alpha$ and edges $e_\alpha^{(ij)} \in \mathcal{E}_\alpha$ where $\mathcal{G}_\alpha = \{\mathcal{V}_\alpha, \mathcal{E}_\alpha\}$. Each node $v_\alpha^{(i)}$ has an associated feature vector $h_\alpha^{(i)}$, and the entire graph has an associated edge attribute tensor $a_\alpha^{(ijr)}$ describing r different relationships between node $v_\alpha^{(i)}$ and its neighbors $v_\alpha^{(j)}$. Here, we can define $\mathcal{N}(i)$ as the set of neighbors of node $v_\alpha^{(i)}$ and take $r = 1$, as we will only consider one edge attribute, i.e. $a_\alpha^{(ijr)} \rightarrow a_\alpha^{(ij)}$. The edge attributes are typically formed from the features corresponding to each node and its neighbors.

In the layer structure of a GNN, multilayer perceptions (MLPs) are used to update the node features and edge attributes before aggregating, or mean pooling, the updated node features for each graph to make a final prediction. To simplify notation, we will omit the graph index α , lower the node index i , and introduce a model layer index l . The first MLP is the edge MLP ϕ_e which, at each layer l ,

collects the features \mathbf{h}_i^l , its neighbors' features \mathbf{h}_j^l , and the edge attribute a_{ij} corresponding to the pair. Once the new edge matrix m_{ij} is formed, we sum along the neighbor dimension j to create a new node feature \mathbf{m}_i . This extra feature is then added to the original node features \mathbf{h}_i before being input into a second node updating MLP ϕ_h to form new node features \mathbf{h}_i^{l+1} [15, 14, 30]. Therefore, a GNN is defined as

$$\mathbf{m}_{ij} = \phi_e(\mathbf{h}_i^l, \mathbf{h}_j^l, a_{ij}), \quad (5a)$$

$$\mathbf{m}_i = \sum_{j \in \mathcal{N}(i)} \mathbf{m}_{ij}, \quad (5b)$$

$$\mathbf{h}_i^{l+1} = \phi_h(\mathbf{h}_i^l, \mathbf{m}_i). \quad (5c)$$

Here, $\mathbf{h}_i^l \in \mathbb{R}^k$ is the k -th dimensional embedding of node v_i at layer l and \mathbf{m}_{ij} is typically referred to as the message passing function. Once the data is sent through the P graph layers of the GNN, the updated nodes \mathbf{h}_i^P are aggregated via mean pooling for each graph to form a set of final features $\frac{1}{n_\alpha} \sum_{i=1}^{n_\alpha} \mathbf{h}_i^P$. These final features are sent through a fully connected neural network (NN) to output the predictions. Typically, a fixed number of hidden features $k = N_h$ is defined for both the edge and node MLPs. The described GNN architecture is pictorially shown in the left panel of Fig. 3.

3.3 SE(2) equivariant graph neural network

For the classical EGNN, the approach used here was informed by the successful implementation of SE(3), or rotational, translational, and permutational, equivariance on dynamical systems and the QM9 molecular dataset [30]. It should be noted that GNNs are naturally permutation equivariant, in particular invariant, when averaging over the final node feature outputs of the graph layers [35]. An SE(2) EGNN takes the same form as a GNN, however, the coordinates are equivariantly updated within each graph layer, i.e. $\mathbf{x}_i \rightarrow \mathbf{x}_i^l$ where $\mathbf{x}_i = (\phi_i, y_i)$ in our case. The new form of the network becomes

$$\mathbf{m}_{ij} = \phi_e(\mathbf{h}_i^l, \mathbf{h}_j^l, a_{ij}, |\mathbf{x}_i^l - \mathbf{x}_j^l|), \quad (6a)$$

$$\mathbf{m}_i = \sum_{j \in \mathcal{N}(i)} \mathbf{m}_{ij}, \quad (6b)$$

$$\mathbf{x}_i^{l+1} = \mathbf{x}_i^l + C \sum_{j \neq i} (\mathbf{x}_i^l - \mathbf{x}_j^l) \phi_x(\mathbf{m}_{ij}), \quad (6c)$$

$$\mathbf{h}_i^{l+1} = \phi_h(\mathbf{h}_i^l, \mathbf{m}_i). \quad (6d)$$

Since the coordinates \mathbf{x}_i^l of each node v_i are equivariantly evolving, we also introduce a second invariant embedding $|\mathbf{x}_i^l - \mathbf{x}_j^l|$ based on the equivariant coordinates into the edge MLP ϕ_e . The coordinates \mathbf{x}_i are updated by adding the summed difference between coordinate \mathbf{x}_i and its neighbors \mathbf{x}_j where the added term is enhanced by a factor of C , which we take as $C = \frac{1}{\ln(2n_\alpha)}$, and a coordinate MLP ϕ_x which takes as input the message passing function \mathbf{m}_{ij} . For a proof on the rotational and translational equivariance of \mathbf{x}_i^{l+1} , see Appendix A. The described EGNN architecture is pictorially shown in the right panel of Fig. 3.

3.4 Quantum graph neural network

For a QGNN, the input data, as a collection of graphs $\{\mathcal{G}_\alpha\}$, is the same as described above. We fix the number of qubits n to be the number of nodes n_α in each graph. For the quantum algorithm, we first form a normalized qubit product state from an embedding MLP $\phi_{|\psi^0\rangle}$ which takes in the features \mathbf{h}_i of each node v_i and reduces each of them to a qubit state $|\phi_{|\psi^0\rangle}(\mathbf{h}_i)\rangle \in \mathbb{C}^2$ [20]. The initial product state describing the system then becomes $|\psi_\alpha^0\rangle = \bigotimes_{i=1}^n |\phi_{|\psi\rangle}(\mathbf{h}_i)\rangle \in \mathbb{C}^{2^n}$, which we normalize by $\sqrt{\langle \psi_\alpha^0 | \psi_\alpha^0 \rangle}$.

A fully parameterized Hamiltonian can then be constructed based on the adjacency matrix a_{ij} and node features \mathbf{h}_i or trainable interaction \mathcal{W}_{ij} and feature \mathcal{M}_i weights [38]. Here, for the coupling term of the Hamiltonian H_C , we utilize the edge matrix a_{ij} connected to two coupled Pauli-Z operators, σ_i^z and σ_j^z , which act on the Hilbert spaces of qubits i and j , respectively. Since we embed

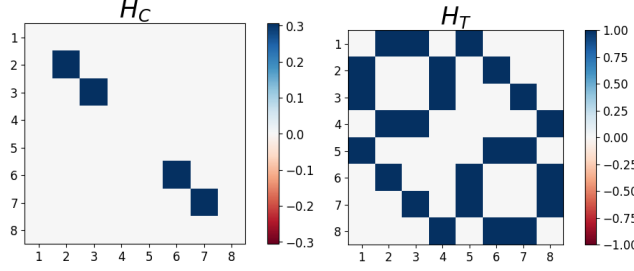


Figure 5: 8×8 matrix representations of the coupling and transverse Hamiltonians defined in Eq. (7).

the quantum state $|\psi^0\rangle$ based on the node features \mathbf{h}_i , we omit the self-interaction term, which utilizes the chosen features applied to the Pauli-Z operator, σ_i^z , acting on the Hilbert space of qubit i . We also introduce a transverse term H_T to each node in the form of a Pauli-X operator, σ_i^x with a fixed or learnable constant coefficient \mathcal{Q}_0 , which we take to be $\mathcal{Q}_0 = 1$. Note that the Hamiltonian H contains $\mathcal{O}(2^n \times 2^n)$ entries due to the Kronecker products between Pauli operators. To best express the properties of each graph, we take the Hamiltonian of the form

$$H(a_{ij}) = \underbrace{\sum_{(i,j) \in \mathcal{E}} a_{ij} \left(\frac{\hat{\mathbb{I}}_i - \sigma_i^z}{2} - \frac{\hat{\mathbb{I}}_j - \sigma_j^z}{2} \right)^2}_{H_C} + \underbrace{\sum_{i \in \mathcal{V}} \sigma_i^x}_{H_T}, \quad (7)$$

where the 8×8 matrix representations of H_C and H_T are shown in Fig. 5. We generate the unitary form of the operator by complex exponentiating the Hamiltonian with real learnable coefficients $\gamma_{lq} \in \mathbb{R}^{P \times Q}$, which can be thought of as infinitesimal parameters running over $Q = 2$ Hamiltonian terms and P layers of the network. Therefore, the QGNN can be defined as

$$U_{ij} = \phi_u(a_{ij}) = e^{-i \sum_{q=1}^Q \gamma_{lq} H_q(a_{ij})}, \quad (8a)$$

$$|\psi^{l+1}\rangle = \phi_{|\psi}\rangle(|\psi^l\rangle, U_{ij}) = U_\theta^l U_{ij} U_\theta^{l\dagger} |\psi^l\rangle, \quad (8b)$$

where $U_\theta^l = (\theta' - i\mathbb{I})(\theta' + i\mathbb{I})^{-1}$ is a parameterized unitary Cayley transformation in which we force $\theta' = \theta + \theta^\dagger$ to be self-adjoint, i.e. $\theta' = \theta'^\dagger$, with $\theta \in \mathbb{C}^{2^n \times 2^n}$ as the trainable parameters. The QGNN evolves the quantum state $|\psi^0\rangle$ by applying unitarily transformed ansatz Hamiltonians with Q terms to the state over P layers. The final product state $|\psi^P\rangle \in \mathbb{C}^{2^n}$ is measured for output which is sent to a classical fully connected NN to make a prediction. The analogy between the quantum unitary interaction function ϕ_u and classical edge MLP ϕ_e , as well as, between the quantum unitary state update function $\phi_{|\psi}\rangle$ and classical node update function ϕ_h should be clear. For a reduction of the coupling Hamiltonian H_C in Eq. (7), see Appendix B. The described QGNN architecture is pictorially shown in the left panel of Fig. 4.

3.5 Permutation equivariant quantum graph neural Network

The EQGNN takes the same form as the QGNN, however, we aggregate the final elements of the product state $\frac{1}{2^n} \sum_{k=1}^{2^n} |\psi_k^P\rangle$ via mean pooling before sending this complex value to a fully connected NN [26, 20, 34]. See appendix C for a proof of the quantum product state permutation equivariance over the sum of its elements. The resulting EQGNN architecture is shown in the right panel of Fig. 4.

4 Results and Analysis

For each model, a range of total parameters were tested, however, the overall comparison test was done using the largest optimal number of total parameters for each network. A feed forward NN was used to reduce each network's graph layered output to a binary one followed by the softmax activation function to obtain the logits in the classical case and the norm of the complex values to obtain the logits in the quantum case. Each model trained over 20 epochs with the Adam optimizer consisting of a learning rate of $\eta = 10^{-3}$ and a cross-entropy loss function. The classical networks

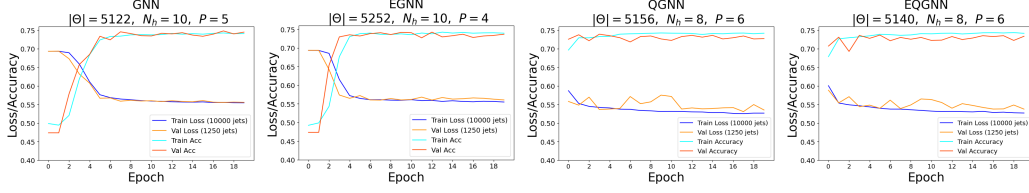


Figure 6: (a) GNN, (b) EGNN, (c) QGNN, and (d) EQGNN training history plots.

Table 1: Metric comparison between the classical and quantum graph models.

Model	$ \Theta $	N_h	P	Train ACC	Val ACC	Test AUC
GNN	5122	10	5	74.25%	74.80%	63.36%
EGNN	5252	10	4	73.66%	74.08%	67.88%
QGNN	5156	8	6	74.00%	73.28%	61.43%
EQGNN	5140	8	6	74.42%	72.56%	75.17%

trained with a batch size of 64 and the quantum networks with a batch size of one due to the limited capabilities of broadcasting unitary operators in the quantum APIs. The best model weights were saved when the validation AUC, or area under the curve of the true positive rate (TPR) as a function of the false positive rate (FPR), was maximized after epoch 15. The results of the training for the largest optimal total number of parameters $|\Theta| \approx 5100$ can be seen in Fig. 6 with more details listed in Table 1. Recall that for each model, we vary the number of hidden features N_h in the P graph layers. Since we fix the number of nodes $n_\alpha = 3$ per jet, the hidden feature number $N_h = 2^3 = 8$ becomes fixed in the quantum case, and therefore, we also varied the parameters of the encoder $\phi_{|\psi\rangle\phi\rangle}$ and decoder NN in the quantum algorithms.

Based on the AUC scores, the EGNN outperformed both the classical and quantum GNN, however, this algorithm was outperformed by the EQGNN with a 7.29% increase in AUC representing the strength of the EQGNN. Although the GNN outperformed the QGNN in the final parameter test by 1.93%, the QGNN performed more consistently and outperformed the GNN in the mid parameter range $|\Theta| \in (1500, 4000)$. Through the variation of the number of parameters, the AUC scores were recorded for each case where the number of parameters taken for each point corresponds to $|\Theta| \approx \{500, 1200, 1600, 2800, 3500, 5100\}$ as shown in the right panel of Fig. 7.

5 Conclusions

Through several computational experiments, the quantum GNNs seem to exhibit enhanced classifier performance over their classical GNN counterparts based on the best test AUC scores produced after the training of the models while relying on a similar number of parameters, hyperparameters, and model structures. These results seem promising for the quantum advantage over classical models. Despite this result, the quantum algorithms take over 100 times as long to train than the classical networks. This may be attributed to the limited capabilities in the quantum APIs, where the inability

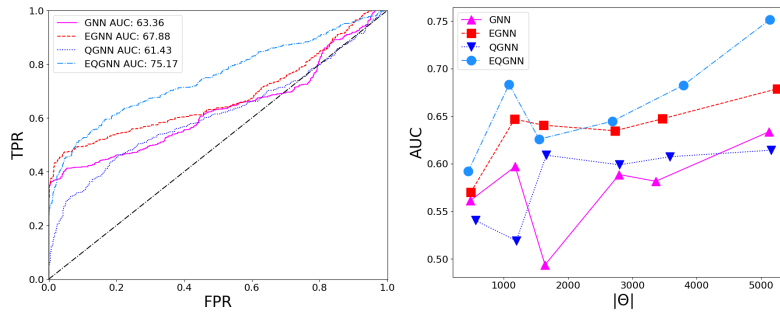


Figure 7: Model ROC curves (left) and AUC scores as a function of parameters (right).

to train with broadcastable unitary operators forced the quantum models to take in a batch size of one, or train on a single graph at a time.

The action of the equivariance in the EGNN and EQGNN could be further explored and developed. This is especially true in the quantum case where more general permutation and $SU(2)$ equivariance have been explored [34, 20, 6, 40]. Expanding the flexibility of the networks to an arbitrary number of nodes per graph should also offer increased robustness, however, this may continue to pose challenges in the quantum case due to the current limited flexibility of quantum software. A variety of different forms of the networks can also be explored, such as introducing attention components and altering the structure of the quantum graph layers to achieve enhanced performance of both classical and quantum GNNs. In particular, one can further parameterize the quantum graph layer structure to better align with the total number of parameters used in the classical structures. These avenues will be explored in future work.

6 Software and Code

PyTorch and PennyLane were the primary APIs used in the formation and testing of these algorithms. The code corresponding to this paper can be found at GitHub - royforestano.

Acknowledgements

This research used resources of the National Energy Research Scientific Computing Center, a DOE Office of Science User Facility supported by the Office of Science of the U.S. Department of Energy under Contract No. DE-AC02-05CH11231 using NERSC award NERSC DDR-ERCAP0025759. SG is supported in part by the U.S. Department of Energy (DOE) under Award No. DE-SC0012447. KM is supported in part by the U.S. DOE award number DE-SC0022148. KK is supported in part by US DOE DE-SC0024407. CD is supported in part by College of Liberal Arts and Sciences Research Fund at the University of Kansas. CD, RF, EU, MCC and TM were participants in the 2023 Google Summer of Code.

References

- [1] X. Ai, Z. Zhang, L. Sun, J. Yan, and E. R. Hancock. Decompositional quantum graph neural network. *CoRR*, abs/2201.05158, 2022.
- [2] A. Andreassen, I. Feige, C. Frye, and M. D. Schwartz. JUNIPR: a framework for unsupervised machine learning in particle physics. *The European Physical Journal C*, 79(2), feb 2019. doi: 10.1140/epjc/s10052-019-6607-9. URL <https://doi.org/10.1140%2Fepjc%2Fs10052-019-6607-9>.
- [3] K. Beer, M. Khosla, J. Köhler, T. J. Osborne, and T. Zhao. Quantum machine learning of graph-structured data. *Phys. Rev. A*, 108:012410, Jul 2023. doi: 10.1103/PhysRevA.108.012410. URL <https://link.aps.org/doi/10.1103/PhysRevA.108.012410>.
- [4] E. A. Cherrat, I. Kerenidis, N. Mathur, J. Landman, M. C. Strahm, and Y. Y. Li. Quantum vision transformers, 2023. URL <https://openreview.net/forum?id=p7xPXoKBOH>.
- [5] C. Chu, G. Skipper, M. Swamy, and F. Chen. Iqgan: Robust quantum generative adversarial network for image synthesis on nisq devices. In *ICASSP 2023 - 2023 IEEE International Conference on Acoustics, Speech and Signal Processing (ICASSP)*, pages 1–5, 2023. doi: 10.1109/ICASSP49357.2023.10096772.
- [6] R. D. P. East, G. Alonso-Linaje, and C.-Y. Park. All you need is spin: $SU(2)$ equivariant variational quantum circuits based on spin networks, 2023.
- [7] A. S. Ecker, F. H. Sinz, E. Froudarakis, P. G. Fahey, S. A. Cadena, E. Y. Walker, E. Cobos, J. Reimer, A. S. Tolias, and M. Bethge. A rotation-equivariant convolutional neural network model of primary visual cortex. In *International Conference on Learning Representations*, 2019. URL <https://openreview.net/forum?id=H1fU8iAqKX>.

- [8] C. Esteves. Theoretical aspects of group equivariant neural networks, 2020.
- [9] R. T. Forestano, K. T. Matchev, K. Matcheva, A. Roman, E. B. Unlu, and S. Verner. Identifying the Group-Theoretic Structure of Machine-Learned Symmetries. 9 2023.
- [10] R. T. Forestano, K. T. Matchev, K. Matcheva, A. Roman, E. B. Unlu, and S. Verner. Deep learning symmetries and their Lie groups, algebras, and subalgebras from first principles. *Mach. Learn. Sci. Tech.*, 4(2):025027, 2023. doi: 10.1088/2632-2153/acd989.
- [11] R. T. Forestano, K. T. Matchev, K. Matcheva, A. Roman, E. B. Unlu, and S. Verner. Accelerated Discovery of Machine-Learned Symmetries: Deriving the Exceptional Lie Groups G₂, F₄ and E₆. 7 2023.
- [12] R. T. Forestano, K. T. Matchev, K. Matcheva, A. Roman, E. B. Unlu, and S. Verner. Discovering Sparse Representations of Lie Groups with Machine Learning. *Physics Letters B*, 844, 9 2023. doi: 10.1016/j.physletb.2023.138086.
- [13] R. Franceschini, D. Kim, K. Kong, K. T. Matchev, M. Park, and P. Shyamsundar. Kinematic Variables and Feature Engineering for Particle Phenomenology. 6 2022.
- [14] J. Gilmer, S. S. Schoenholz, P. F. Riley, O. Vinyals, and G. E. Dahl. Neural message passing for quantum chemistry. In D. Precup and Y. W. Teh, editors, *Proceedings of the 34th International Conference on Machine Learning*, volume 70 of *Proceedings of Machine Learning Research*, pages 1263–1272. PMLR, 06–11 Aug 2017. URL <https://proceedings.mlr.press/v70/gilmer17a.html>.
- [15] T. N. Kipf and M. Welling. Semi-supervised classification with graph convolutional networks. *arXiv preprint arXiv:1609.02907*, 2016.
- [16] T. N. Kipf and M. Welling. Semi-Supervised Classification with Graph Convolutional Networks. In *Proceedings of the 5th International Conference on Learning Representations*, ICLR ’17, 2017. URL <https://openreview.net/forum?id=SJU4ayYgl>.
- [17] P. T. Komiske, E. M. Metodiev, and J. Thaler. Energy flow networks: deep sets for particle jets. *Journal of High Energy Physics*, 2019(1), jan 2019. doi: 10.1007/jhep01(2019)121. URL <https://doi.org/10.1007%2Fjhep01%282019%29121>.
- [18] L. Lim and B. J. Nelson. What is an equivariant neural network? *CoRR*, abs/2205.07362, 2022. doi: 10.48550/arXiv.2205.07362. URL <https://doi.org/10.48550/arXiv.2205.07362>.
- [19] H. Maron, H. Ben-Hamu, N. Shamir, and Y. Lipman. Invariant and equivariant graph networks. In *International Conference on Learning Representations*, 2019. URL <https://openreview.net/forum?id=Syx72jC9tm>.
- [20] P. Mernyei, K. Meichanetzidis, and İsmail İlkan Ceylan. Equivariant quantum graph circuits, 2022.
- [21] J. J. Meyer, M. Mularski, E. Gil-Fuster, A. A. Mele, F. Arzani, A. Wilms, and J. Eisert. Exploiting symmetry in variational quantum machine learning. *PRX Quantum*, 4(1), mar 2023. doi: 10.1103/prxquantum.4.010328. URL <https://doi.org/10.1103%2Fprxquantum.4.010328>.
- [22] V. Mikuni and F. Canelli. Abcnet: an attention-based method for particle tagging. *The European Physical Journal Plus*, 135(6):463, 2020. doi: 10.1140/epjp/s13360-020-00497-3. URL <https://doi.org/10.1140/epjp/s13360-020-00497-3>.
- [23] V. Mikuni and F. Canelli. Point cloud transformers applied to collider physics. *Machine Learning: Science and Technology*, 2(3):035027, jul 2021. doi: 10.1088/2632-2153/ac07f6. URL <https://doi.org/10.1088%2F2632-2153%2Fac07f6>.
- [24] F. Mokhtar, R. Kansal, and J. Duarte. Do graph neural networks learn traditional jet substructure? In *36th Conference on Neural Information Processing Systems*, 11 2022.
- [25] D. Murnane, S. Thais, and A. Thete. Equivariant graph neural networks for charged particle tracking, 2023.

- [26] Q. T. Nguyen, L. Schatzki, P. Braccia, M. Ragone, P. J. Coles, F. Sauvage, M. Larocca, and M. Cerezo. Theory for equivariant quantum neural networks. *ArXiv*, abs/2210.08566, 2022. URL <https://api.semanticscholar.org/CorpusID:252917789>.
- [27] M. Y. Niu, A. Zlokapa, M. Broughton, S. Boixo, M. Mohseni, V. Smelyanskiy, and H. Neven. Entangling Quantum Generative Adversarial Networks. *Phys. Rev. Lett.*, 128(22):220505, 2022. doi: 10.1103/PhysRevLett.128.220505.
- [28] E. Rodrigues and H. Schreiner. scikit-hep/particle: Version 0.23.0, July 2023. URL <https://doi.org/10.5281/zenodo.8112280>.
- [29] A. Roman, R. T. Forestano, K. T. Matchev, K. Matcheva, and E. B. Unlu. Oracle-preserving latent flows. *Symmetry*, 15(7), 2023. ISSN 2073-8994. doi: 10.3390/sym15071352. URL <https://www.mdpi.com/2073-8994/15/7/1352>.
- [30] V. G. Satorras, E. Hoogeboom, and M. Welling. E(n) equivariant graph neural networks. *ArXiv*, abs/2102.09844, 2021. URL <https://api.semanticscholar.org/CorpusID:231979049>.
- [31] L. Schatzki, M. Larocca, Q. T. Nguyen, F. Sauvage, and M. Cerezo. Theoretical guarantees for permutation-equivariant quantum neural networks, 2022.
- [32] J. Shlomi, P. Battaglia, and J.-R. Vlimant. Graph neural networks in particle physics. *Machine Learning: Science and Technology*, 2(2):021001, Dec 2020. doi: 10.1088/2632-2153/abbb9a. URL <https://dx.doi.org/10.1088/2632-2153/abbb9a>.
- [33] R. D. Sipio, J.-H. Huang, S. Y.-C. Chen, S. Mangini, and M. Worring. The dawn of quantum natural language processing. *ICASSP 2022 - 2022 IEEE International Conference on Acoustics, Speech and Signal Processing (ICASSP)*, pages 8612–8616, 2021. URL <https://api.semanticscholar.org/CorpusID:238744248>.
- [34] A. Skolik, M. Cattelan, S. Yarkoni, T. Bäck, and V. Dunjko. Equivariant quantum circuits for learning on weighted graphs. *npj Quantum Information*, 9(1):47, 2023. doi: 10.1038/s41534-023-00710-y. URL <https://doi.org/10.1038/s41534-023-00710-y>.
- [35] E. H. Thiede, T. S. Hy, and R. Kondor. The general theory of permutation equivariant neural networks and higher order graph variational encoders, 2020.
- [36] P. Veličković. Everything is connected: Graph neural networks. *Current Opinion in Structural Biology*, 79:102538, 2023. ISSN 0959-440X. doi: <https://doi.org/10.1016/j.sbi.2023.102538>. URL <https://www.sciencedirect.com/science/article/pii/S0959440X2300012X>.
- [37] P. Veličković, G. Cucurull, A. Casanova, A. Romero, P. Liò, and Y. Bengio. Graph attention networks. In *International Conference on Learning Representations*, 2018. URL <https://openreview.net/forum?id=rJXMpikCZ>.
- [38] G. Verdon, T. Mccourt, E. Luzhnica, V. Singh, S. Leichenauer, and J. D. Hidary. Quantum graph neural networks. *ArXiv*, abs/1909.12264, 2019. URL <https://api.semanticscholar.org/CorpusID:202889158>.
- [39] D. E. Worrall, S. J. Garbin, D. Turmukhambetov, and G. J. Brostow. Harmonic networks: Deep translation and rotation equivariance. In *2017 IEEE Conference on Computer Vision and Pattern Recognition (CVPR)*, pages 7168–7177, Los Alamitos, CA, USA, jul 2017. IEEE Computer Society. doi: 10.1109/CVPR.2017.758. URL <https://doi.ieeecomputersociety.org/10.1109/CVPR.2017.758>.
- [40] H. Zheng, C. Kang, G. S. Ravi, H. Wang, K. Setia, F. T. Chong, and J. Liu. Sncqa: A hardware-efficient equivariant quantum convolutional circuit architecture, 2023.
- [41] J. Zhou, G. Cui, S. Hu, Z. Zhang, C. Yang, Z. Liu, L. Wang, C. Li, and M. Sun. Graph neural networks: A review of methods and applications. *AI Open*, 1:57–81, 2020. ISSN 2666-6510. doi: <https://doi.org/10.1016/j.aiopen.2021.01.001>. URL <https://www.sciencedirect.com/science/article/pii/S2666651021000012>.

A Equivariant coordinate update function

Let $T_g : X \rightarrow X$ be the set of translational and rotational group transformations with elements $g \in T_g \subset G$ which act on the vector space X . The function $\varphi : X \rightarrow X$ defined by

$$\varphi(x) = x_i + C \sum_{j \neq i} (x_i - x_j) \quad (9)$$

is equivariant with respect to T_g .

Proof. Let a general transformation $g \in T_g$ act on X by $gX = RX + T$, where $R \in T_g$ denotes a general rotation and $T \in T_g$ a general translation. Then, under the transformation g on X of the function φ defined above, we have

$$\begin{aligned} \varphi(gx) &= (gx_i) + C \sum_{j \neq i} (gx_i - gx_j) \\ &= (Qx_i + T) + C \sum_{j \neq i} (Qx_i + T - Qx_j - T) \\ &= (Qx_i + T) + C \sum_{j \neq i} (Qx_i - Qx_j) \\ &= Qx_i + C \sum_{j \neq i} Q(x_i - x_j) + T \\ &= Q[x_i + C \sum_{j \neq i} (x_i - x_j)] + T \\ &= g\varphi(x), \end{aligned}$$

where $\varphi(gx) = g\varphi(x)$ shows φ transforms equivariantly under transformations $g \in T_g$ acting on X . \square

B Coupling Hamiltonian simplification

The reduction of the coupling Hamiltonian becomes

$$\begin{aligned} \hat{H}_C &= \frac{1}{2} \sum_{(j,k) \in \mathcal{E}} \Lambda_{jk} \left[\left(\frac{\hat{I}_j - \sigma_j^z}{2} \right) - \left(\frac{\hat{I}_k - \sigma_k^z}{2} \right) \right]^2 \\ &= \frac{1}{8} \sum_{(j,k) \in \mathcal{E}} \Lambda_{jk} \left[(\hat{I}_j - \sigma_j^z) - (\hat{I}_k - \sigma_k^z) \right]^2 \\ &= \frac{1}{8} \sum_{(j,k) \in \mathcal{E}} \Lambda_{jk} \left[(\hat{I}_j - \sigma_j^z)^2 - (\hat{I}_j - \sigma_j^z)(\hat{I}_k - \sigma_k^z) - (\hat{I}_k - \sigma_k^z)(\hat{I}_j - \sigma_j^z) + (\hat{I}_k - \sigma_k^z)^2 \right] \\ &= \frac{1}{8} \sum_{(j,k) \in \mathcal{E}} \Lambda_{jk} \left[\hat{I}_j \hat{I}_j - \hat{I}_j \sigma_j^z - \sigma_j^z \hat{I}_j + \sigma_j^z \sigma_j^z - \hat{I}_j \hat{I}_k + \hat{I}_j \sigma_k^z + \sigma_j^z \hat{I}_k - \sigma_j^z \sigma_k^z - \hat{I}_k \hat{I}_j + \hat{I}_k \sigma_j^z + \sigma_k^z \hat{I}_j \right. \\ &\quad \left. - \sigma_k^z \sigma_j^z + \hat{I}_k \hat{I}_k - \hat{I}_k \sigma_k^z - \sigma_k^z \hat{I}_k + \sigma_k^z \sigma_k^z \right] \\ &= \frac{1}{8} \sum_{(j,k) \in \mathcal{E}} \Lambda_{jk} \left[\hat{I}_j \hat{I}_j - 2\hat{I}_j \sigma_j^z + \sigma_j^z \sigma_j^z - 2\hat{I}_j \hat{I}_k + 2\hat{I}_j \sigma_k^z + 2\sigma_j^z \hat{I}_k - 2\sigma_j^z \sigma_k^z + \hat{I}_k \hat{I}_k - 2\hat{I}_k \sigma_k^z + \sigma_k^z \sigma_k^z \right] \\ &= \frac{1}{8} \sum_{(j,k) \in \mathcal{E}} \Lambda_{jk} \left[\hat{I}_j - 2\sigma_j^z + \sigma_j^{z2} - 2\hat{I}_j \hat{I}_k + 2\hat{I}_j \sigma_k^z + 2\sigma_j^z \hat{I}_k - 2\sigma_j^z \sigma_k^z + \hat{I}_k - 2\sigma_k^z + \sigma_k^{z2} \right] \\ &= \frac{1}{8} \sum_{(j,k) \in \mathcal{E}} \Lambda_{jk} \left[2\hat{I}_j - 2\sigma_j^z - 2\hat{I}_j \hat{I}_k + 2\hat{I}_j \sigma_k^z + 2\sigma_j^z \hat{I}_k - 2\sigma_j^z \sigma_k^z + 2\hat{I}_k - 2\sigma_k^z \right] \end{aligned}$$

$$= \frac{1}{4} \sum_{(j,k) \in \mathcal{E}} \Lambda_{jk} \left[\hat{I}_j - \sigma_j^z - \hat{I}_j \hat{I}_k + \hat{I}_j \sigma_k^z + \sigma_j^z \hat{I}_k - \sigma_j^z \sigma_k^z + \hat{I}_k - \sigma_k^z \right],$$

and multiplying on the left by \hat{I}_j and on the right by \hat{I}_k admits

$$\begin{aligned} \Rightarrow \hat{H}_C &= \frac{1}{4} \sum_{(j,k) \in \mathcal{E}} \Lambda_{jk} \left[\hat{I}_j \hat{I}_k - \sigma_j^z \hat{I}_k + \hat{I}_j \sigma_k^z + \sigma_j^z \hat{I}_k - \sigma_j^z \sigma_k^z - \hat{I}_j \sigma_k^z \right] \\ &= \frac{1}{4} \sum_{(j,k) \in \mathcal{E}} \Lambda_{jk} \left[\hat{I}_j \hat{I}_k - \sigma_j^z \sigma_k^z \right]. \end{aligned} \quad (10)$$

C Quantum product state permutation equivariance

For V a commutable vector space, the product state $\bigotimes_{i=1}^m \mathbf{v}_i : V^n \times \dots \times V^n \rightarrow V^{n^m}$ is permutation equivariant with respect to the sum of its entries. We prove the $n = 2$ case for all $m \in \mathbb{Z}_{>0}$.

Proof. (By Induction) Assume we have $n = 1$ final qubit state,

$$|\psi_1\rangle = \bigotimes_{i=1}^1 \begin{pmatrix} v_1^1 \\ v_1^2 \end{pmatrix} = \begin{pmatrix} v_1^1 \\ v_1^2 \end{pmatrix},$$

the sum of the product state elements will be trivially equivariant with respect to similar graphs. If we have $n = 2$ final qubit states, the product state is

$$|\psi_i\rangle = \bigotimes_{i=\{1,2\}} \begin{pmatrix} v_i^1 \\ v_i^2 \end{pmatrix} = \begin{pmatrix} v_1^1 \\ v_1^2 \end{pmatrix} \otimes \begin{pmatrix} v_2^1 \\ v_2^2 \end{pmatrix} = \begin{pmatrix} v_1^1 v_2^1 \\ v_1^2 v_2^1 \\ v_1^1 v_2^2 \\ v_1^2 v_2^2 \end{pmatrix},$$

where the sum of elements becomes

$$\begin{aligned} v_1^1 v_2^1 + v_1^2 v_2^1 + v_1^1 v_2^2 + v_1^2 v_2^2 &= v_2^1 v_1^1 + v_2^1 v_1^2 + v_2^2 v_1^1 + v_2^2 v_1^2 \\ &= v_2^1 v_1^1 + v_2^2 v_1^1 + v_2^1 v_1^2 + v_2^2 v_1^2, \end{aligned}$$

which is equivalent to the sum of the elements

$$\begin{pmatrix} v_2^1 v_1^1 \\ v_2^2 v_1^1 \\ v_2^1 v_1^2 \\ v_2^2 v_1^2 \end{pmatrix} = \begin{pmatrix} v_2^1 \\ v_2^2 \end{pmatrix} \otimes \begin{pmatrix} v_1^1 \\ v_1^2 \end{pmatrix} = \bigotimes_{i=\{2,1\}} \begin{pmatrix} v_i^1 \\ v_i^2 \end{pmatrix}$$

for commutative spaces where $v_i^j \in \mathbb{C}$ and $\{1, 2\}, \{2, 1\}$ should be regarded as ordered sets, which again shows the sum of the state elements remaining unchanged when the qubit states switch positions in the product. We will now assume the statement is true for $n = N$ final qubit states and proceed to show the $N + 1$ case is true. The quantum product state over N elements becomes

$$\bigotimes_{i=1}^N |\psi_i\rangle = \bigotimes_i \begin{pmatrix} v_i^1 \\ v_i^2 \end{pmatrix} = \begin{pmatrix} v_1^1 \\ v_1^2 \end{pmatrix} \otimes \begin{pmatrix} v_2^1 \\ v_2^2 \end{pmatrix} \otimes \dots \otimes \begin{pmatrix} v_N^1 \\ v_N^2 \end{pmatrix}, \quad (11)$$

which we assume to be permutation equivariant over the sum of its elements. We can rewrite the form of this state as

$$\bigotimes_{i=1}^N |\psi_i\rangle = \begin{pmatrix} A_1 \\ A_2 \\ \vdots \\ A_{2^N} \end{pmatrix} = A_j, \quad (12)$$

where A_j define the 2^N terms in the final product state. Replacing the $i + 1$ -th entry of the Kronecker product above with a new $N + 1$ -th state, we have

$$\bigotimes_{i=1}^{N+1} |\psi_i\rangle = \bigotimes_i \begin{pmatrix} v_i^1 \\ v_i^2 \end{pmatrix} = \underbrace{\begin{pmatrix} v_1^1 \\ v_1^2 \end{pmatrix} \otimes \begin{pmatrix} v_2^1 \\ v_2^2 \end{pmatrix} \otimes \dots \otimes \begin{pmatrix} v_i^1 \\ v_i^2 \end{pmatrix} \otimes \begin{pmatrix} v_{N+1}^1 \\ v_{N+1}^2 \end{pmatrix} \otimes \begin{pmatrix} v_{i+1}^1 \\ v_{i+1}^2 \end{pmatrix} \otimes \dots \otimes \begin{pmatrix} v_N^1 \\ v_N^2 \end{pmatrix}}_{N+1 \text{ terms}}.$$

When this occurs, this new state consisting of 2^{N+1} elements with the $N + 1$ state in the $i + 1$ -th entry of the product can be written in terms of the old state with groupings of the new elements in 2^{N+1-i} batches of 2^i elements, i.e.

$$\bigotimes_{i=1}^{N+1} |\psi_i\rangle = \begin{pmatrix} B_1 = A_1 v_{N+1}^1 \\ B_2 = A_2 v_{N+1}^1 \\ \vdots \\ B_{2^i} = A_{2^i} v_{N+1}^1 \\ B_{2^i+1} = A_1 v_{N+1}^2 \\ \vdots \\ B_{2^{i+1}} = A_{2^i} v_{N+1}^2 \\ \vdots \\ B_{2^{N+1}-2^{i+1}+1} = A_{2^N-2^i+1} v_{N+1}^1 \\ \vdots \\ B_{2^{N+1}-2^i} = A_{2^N} v_{N+1}^1 \\ B_{2^{N+1}-2^i+1} = A_{2^N-2^i+1} v_{N+1}^2 \\ \vdots \\ B_{2^{N+1}} = A_{2^N} v_{N+1}^2 \end{pmatrix}, \quad (13)$$

which when summed becomes

$$\begin{aligned} \sum_{k=1}^{2^{N+1}} B_k &= \sum_{j=1}^{2^N} A_j v_{N+1}^1 + \sum_{j=1}^{2^N} A_j v_{N+1}^2 \\ &= (v_{N+1}^1 + v_{N+1}^2) \sum_{j=1}^{2^N} A_j. \end{aligned}$$

However, the $i + 1$ -th entry is arbitrary, and due to the summation permutation equivariance of the initial state $\bigotimes_{i=1}^N |\psi_i\rangle$, the sum $\sum_{j=1}^{2^N} A_j$ is equivariant, in fact invariant, under all reorderings of the elements $|\psi_i\rangle$ in the product $\bigotimes_{i=1}^N |\psi_i\rangle$. Therefore, we conclude $\bigotimes_{i=1}^{N+1} |\psi_i\rangle$ is permutation equivariant with respect to the sum of its elements. \square

To show a simple illustration of why 13 is true, let us take two initial states and see what happens when we insert a new state between them, i.e. in the 2nd entry in the product. This should lead to $2^{2+1-1} = 2^2 = 4$ groupings of $2^1 = 2$ elements. To begin, we have

$$\begin{pmatrix} v_1^1 \\ v_2^1 \end{pmatrix} \otimes \begin{pmatrix} v_1^1 \\ v_2^1 \end{pmatrix} = \begin{pmatrix} v_1^1 v_1^1 \\ v_1^1 v_2^1 \\ v_2^1 v_1^1 \\ v_2^1 v_2^1 \end{pmatrix} = \begin{pmatrix} A_1 \\ A_2 \\ A_3 \\ A_4 \end{pmatrix},$$

and when we insert the new third state in the 1-th entry of the product above, we have

$$\begin{pmatrix} v_1^1 \\ v_2^1 \end{pmatrix} \otimes \begin{pmatrix} v_3^1 \\ v_2^1 \end{pmatrix} \otimes \begin{pmatrix} v_1^1 \\ v_2^1 \end{pmatrix} = \begin{pmatrix} v_1^1 v_3^1 v_1^1 \\ v_1^1 v_3^1 v_2^1 \\ v_2^1 v_3^1 v_1^1 \\ v_2^1 v_3^1 v_2^1 \\ v_1^1 v_2^1 v_1^1 \\ v_1^1 v_2^1 v_2^1 \\ v_2^1 v_2^1 v_1^1 \\ v_2^1 v_2^1 v_2^1 \end{pmatrix} = \begin{pmatrix} A_1 v_3^1 \\ A_2 v_3^1 \\ A_1 v_3^2 \\ A_2 v_3^2 \\ A_3 v_3^1 \\ A_4 v_3^1 \\ A_3 v_3^2 \\ A_4 v_3^2 \end{pmatrix},$$

which sums to

$$(A_1 + A_2 + A_3 + A_4) v_3^1 + (A_1 + A_2 + A_3 + A_4) v_3^2 = (v_3^1 + v_3^2) \sum_{i=1}^{2^N=2^2=4} A_i.$$